Poly(butylene succinate) reinforced by small amount of grafted nanofibrillated bacterial cellulose: Toughness variability based on nanocomposites preparation method

Hamidah binti Hashim[a], Xiaochao Xia[a] , Hiroshi Kani[b], Shuichiro Seno[b], Feng Li[c], Takuya Isono[c], Takuya Yamamoto[c], Hirofumi Tani[c], Toshifumi Satoh[c,d], and Kenji Tajima[c] *

[a]Graduate School of Chemical Sciences and Engineering, Hokkaido University, Sapporo, 060-8628, Japan

[b]Hokkaido Research Organization, Industrial Research Institute, Sapporo 060-0819, Japan

[c]Faculty of Engineering, Hokkaido University, Sapporo, 060-8628, Japan

[d]ICReDD List-PF, Hokkaido University, N21W10, Kita-ku, Sapporo 001-0021, Japan

E-mail address:

Hamidah binti Hashim: **bintihashim.hamidah.a7@elms.hokudai.ac.jp**; Xiaochao Xia: **xia.x@wustl.edu**; Hiroshi Kani: **kani-hiroshi@hro.or.jp**; Shuichiro Seno: **seno-shuuichirou@hro.or.jp**; Feng Li: **feng.li@eng.hokudai.ac.jp**; Takuya Isono: **isono.t@eng.hokudai.ac.jp**; Takuya Yamamoto: **yamamoto.t@hokudai.ac.jp**; Hirofumi Tani: **tani@eng.hokudai.ac.jp**; Toshifumi Satoh: **satoh@eng.hokudai.ac.jp**

* Corresponding author Kenji Tajima

Tel.: +81(11)-706-6567; fax: +81(11)-706-6567. Email address: ktajima@eng.hokudai.ac.jp Postal address: Faculty of Engineering, Hokkaido University, N13W8, Kita-ku, Sapporo 060-8628, Japan

Abstract

Polybutylene succinate (PBS) is a promising biodegradable polymer; however, its low mechanical performance limits its application. To address this issue, long fiber length nanofibrillated bacterial cellulose (HP-NFBC), produced by a bottom-up process using cellulose-producing bacterium and hydroxypropyl cellulose (HPC) as a dispersing agent was used as reinforcement agent. Hydrophobic moieties were grafted on HP-NFBC surface to increase surface compatibility. Nanocomposites prepared by both solvent casting and melt-kneading were evaluated. By solvent casting, the addition of 0.25 wt% of grafted HP-NFBC increased the toughness by 212%. Melt-kneading revealed an increase in flexural strength and young's modulus. More evident improvement was observed when the nanocomposites were annealed, and the ultimate strength increased by 113% at 2 wt% of grafted HP-NFBC incorporation. Great increased in toughness were achieved only by small incorporation of grafted HP-NFBC. Additionally, compost biodegradation tests were conducted to confirm that the nanocomposites had biodegradability similar to that of PBS.

Keywords:

A. Cellulose; A. Fibres; A. Polymer-matrix composites (PMCs); B. Mechanical properties

1. Introduction

Bioplastics have been intensely researched as alternatives to petroleum-based plastics in recent decades. However, most of these bioplastics have not reached a commercially viable scale because they are only successful at the laboratory level and do not perform as well as petroleum-based plastics [1–5]. For example, polylactic acid (PLA)

is brittle [6,7], polycaprolactone (PCL) has a low modulus [8,9], polyamides have low toughness, and polyhydroxyalkanoates (PHA), such as poly(3-hydroxybutyrate) (P3HB) and poly(3-hydroxyvalerate) (PHV), have poor mechanical properties and heat resistance [10,11]. Therefore, these shortcomings hinder their widespread adoption and underscore the urgent need to develop bioplastics with enhanced mechanical properties and biodegradability to serve environmental protection efforts better.

Polybutylene succinate (PBS), a semi-crystalline biodegradable aliphatic polyester, has been proposed as one of the most attractive alternatives to petroleum-based plastics because of its good thermal stability and processability [12–14]. PBS is often used in packaging materials, mulching film, and compost bags [15–20]. Owing to its good tensile strength, PBS is often blended with polymers such as PLA to improve their mechanical properties; however, a suitable compatibilizer is required to improve the inherently poor interfacial adhesion [21–23]. Adrar et al. [24] reported that with the incorporation of compatibilizer into the PBS/PLA blend, the tensile modulus has increased; however, the elongation at break has greatly decreased. Recently, Junhao et al. [25] incorporated PLA fiber into PBS and the result showed an increase in Young's modulus but the decreased in toughness. Although natural fiber, such as cellulose, could be an excellent reinforcement (filler) material, achieving significant reinforcement is difficult as similar incompatibility issues may cause aggregation owing to the strong hydrophilicity of cellulose [26–28]. Recently, a cellulose-based PBS composite was reported by Platnieks et al, [29] which showed the increased of young's modulus by about two-fold at 20 ℃,; however, at 40 % nanocellulose loading, the tensile strength and elongation at break significantly decreased compared to at 58 % and 90%. Therefore, the interfacial interaction between PBS and fillers is fundamental for reinforcement.

Nanofibrillated bacterial cellulose (NFBC) is a nanosized cellulose fiber produced from low-molecular-weight biomass such as sugars, glycerol, and molasses through a bottom-up process using cellulose-producing bacteria [30]. Owing to its high mechanical strength and purity and long fiber length (>15 μm), NFBC can be utilized as a nanofiller for nanocomposite materials that consist of a matrix and nanomaterials [31,32]. NFBC can be combined with a dispersing agent, such as hydroxypropyl cellulose (HPC), which is an amphiphilic water-soluble cellulose derivative, to produce NFBC with HPC (HP-NFBC), which shows high dispersibility in some polar organic solvents as well as water [33]. Recently, we succeeded in improving the mechanical properties of PCL by adding HPNFBC modified with PCL side chains. The modification of HPNFBC with a polymer that is compatible with the mixed polymer matrix can enhance its mechanical properties [34].

In this study, we aimed to enhance the mechanical performance of PBS by introducing HP-NFBC modified with hydrophobic moieties that mimic the structure of PBS. This modification is intended to improve the dispersion state and interfacial adhesion within the PBS matrix, maximizing the reinforcing effect of the nanofiller. [35–37]. Two types of nanocomposites preparation method were conducted. Their crystallinity, thermal stability, thermal degradation, and mechanical properties were thoroughly investigated. The unique interactions between HP-NFBC, amorphous P(SA-*alt*-BO), and the PBS matrix are discussed to highlight the potential of this approach in advancing the performance of bioplastics.

2. Experimental

List of materials and structural analysis of HPNFBC-g-P(SA-*alt*-BO) and nanocomposites were provided in supporting information.

2.1. Preparation of P(SA-*alt*-BO)-grafted HP-NFBCs via a "grafting-from" method using ROCOP

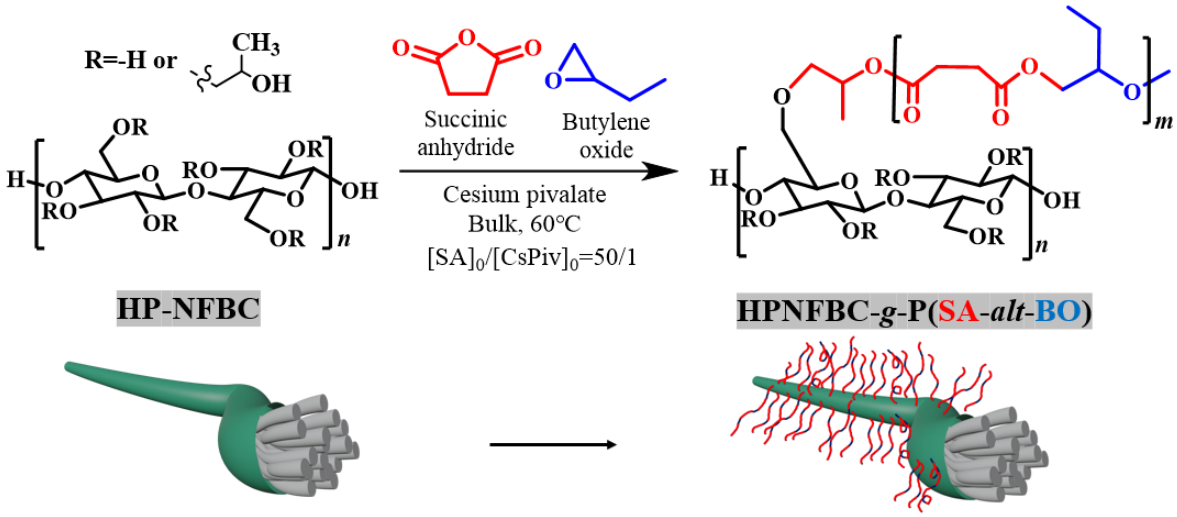

Scheme 1. Preparation of HPNFBC-*g*-P(SA-*alt*-BO) using a "grafting-from" method via ROCOP of succinic anhydride (SA) and 1,2-butylene oxide (BO)

P(SA-*alt*-BO) copolymers were grafted onto HP-NFBC by ROCOP of the SA and BO monomers using cesium pivalate as a catalyst (**Scheme 1**). In an argon-filled glovebox, 0.5 g HP-NFBC was added to a 200 mL round-bottom flask, followed by the addition of monomers, SA (2.5 mmol, 1 equiv.) and BO (0.3 mol, 120 equiv.), and catalyst, cesium pivalate (50µmol, 0.02 equiv.). SA was sublimated and BO was distilled prior to use. 1,3,5-Trimethoxybenzene was used as an internal standard to calculate monomer conversion using proton nuclear magnetic resonance (^{1}H NMR) spectroscopy. The reaction was conducted in bulk at 60 °C with continuous stirring.

Consequently, the solution was diluted by adding an excess amount of CH_2Cl_2 and stirred for 1 d at room temperature for even dispersion before centrifugation. The mixture was then centrifuged (12,000 rpm, 20 °C, 60–90 min) thrice using CH_2Cl_2 to separate

HPNFBC-*g*-P(SA-*alt*-BO) and free P(SA-*alt*-BO). In addition, the mixture was centrifuged using methanol to remove the cesium pivalate catalyst. The HPNFBC-*g*-P(SA-*alt*-BO) was expected to form pellets after centrifugation. The pellet was collected, dispersed in a small amount of CH_2Cl_2 and precipitated in excess hexane to remove impurities. In addition, the free (non-grafted) P(SA-*alt*-BO) copolymer was collected from the filtrate, evaporated, and precipitated in excess hexane. Both the HPNFBC-*g*-P(SA-*alt*-BO) and free P(SA-*alt*-BO) copolymers were dried overnight at room temperature *in vacuo*. The HPNFBC-*g*-P(SA-*alt*-BO) samples with HPNFBC:SA feed weight ratios of 1:80, 1:20, and 1:5 were denoted as HPNFBC-*g*-P(SA-*alt*-BO)-80, HPNFBC-*g*-P(SA-*alt*-BO)-20, and HPNFBC-*g*-P(SA-*alt*-BO)-5, respectively.

2.2. Preparation of HPNFBC-g-P(SA-alt-BO)/PBS nanocomposites

2.2.1. Solvent-casting

PBS pellet was dissolved in 10 mL $CHCl_3$ at 60 °C for 3 h or until fully dissolved. HPNFBC-*g*-P(SA-*alt*-BO) was added to the PBS solution [15 (w/v)%] and stirred at 60 °C for 1 d. The HPNFBC-*g*-P(SA-*alt*-BO)s and PBS compositions were adjusted to prepare nanocomposites containing 0, 0.25, 0.5, 2, and 5 wt% of HPNFBC-*g*-P(SA-*alt*-BO). The solution was cast onto a Teflon Petri dish. A larger glass Petri dish was used as a lid to cover the sample. An additional small glass Petri dish containing $CHCl_3$ was added to the vessel to slow the solvent evaporation rate. A solid film with thickness of 150–250 μm was obtained.

2.2.2. Melt-kneading

PBS resin and HPNFBC-*g*-P(SA-*alt*-BO) were melt-kneaded with a Brabender Plastograph® EC plus mixer at the speed of 80 rpm at 120 °C for 5 min. The mixed blends

were compressed at 150 ℃ using a hot-pressing machine, and cut into 80 × 10 × 2 mm test specimen.

3. Results and Discussions

3.1. Synthesis and structural analysis of HPNFBC-*g*-P(SA-*alt*-BO)s

Synthesis of copolymer P(SA-*alt*-BO) was carried out in bulk with excess BO added as a solvent. The ratio of monomers to HP-NFBC was adjusted to obtain HPNFBC-*g*-P(SA-*alt*-BO) with four copolymer graft lengths. The polymerization reactions were terminated when the SA monomer conversion reached ≥80%. 1,3,5-Trimethoxybenzene was used as an internal standard to precisely determine the monomer conversions by comparing the internal standard peak with the monomer peak before and after the reaction (**Figures S1–S3**). Xia et al. found that electrophilically activated anhydrides are more likely to be attacked by hydroxyl groups to form carboxylates, which then react with epoxides to form fully alternating copolymer structures [38]. In this study, SA reacted with the cesium pivalate-activated hydroxyl group of HP-NFBC to form a carboxylate, which then reacted with BO. The successful formation of alternating P(SA-*alt*-BO) was confirmed by the presence of **c'** and **g** peaks using ^{1}H NMR analysis (**Figure S4**). The accurate molecular weights of the grafted P(SA-*alt*-BO) copolymers in HPNFBC-*g*-P(SA-*alt*-BO) could not be determined because of their poor solubility in solvents for SEC and ^{1}H NMR measurements. In addition, other techniques, including chain cleavage, are unfavorable and complicated [39–41]. Therefore, the length of grafted copolymer was comparatively defined by the length of each free copolymer produced as side reaction during the synthesis of each graft copolymer [42,43]. The molecular weights of the free copolymers increased with the monomer content in the initial compositions (**Figure S5,**

Table 1). When the monomer ratio of SA to HP-NFBC was 80/1, its molecular weight reached 33k, showcasing the significant impact of a high monomer ratio on molecular weight. Similarly, for the 20/1 monomer ratio, the resulting molecular weight was slightly lower at 29k followed by the molecular weight at 5/1 monomer ratio, indicating a proportionate relationship between the monomer ratio and molecular weight.

Table 1 Polymerization conditions and molecular parameters of HPNFBC- g-P(SA-*alt*-BO)s.

Sample	$w_{0,\,SA}$/ $w_{0,\,HP\text{-}NFBC}$[a]	$M_{n,SEC}$[b] of obtained free copolymer [kDa]	M_w / M_n[b]
HPNFBC-*g*-P(SA-*alt*-BO) (33k)	80/1	33,000	1.16
HPNFBC-*g*-P(SA-*alt*-BO) (29k)	20/1	28,900	1.23
HPNFBC-*g*-P(SA-*alt*-BO) (15k)	5/1	14,700	1.37

[a]Mass ratio of SA monomer and HP-NFBC before polymerization; [b]Determined by SEC analysis of the obtained free P(SA-*alt*-BO) copolymers in THF with polystyrene standard. BO: 1,2-butylene oxide; HP-NFBC: hydroxypropyl-nanofibrillated bacterial cellulose; $M_{n,SEC}$: number-average molecular weight; M_w/M_n: narrow molecular weight distribution; SA: succinic anhydride; SEC: size-exclusion chromatography; THF: Tetrahydrofuran.

Overall, the higher the monomer ratio, the greater was the resulting molecular weight, highlighting the controlled reactivity inherent in this copolymerization reaction. This is consistent with the work of Lönnberg et al. [44], who found that the amount of grafted polymer could be controlled by adjusting the ratio of the free initiator to the monomer. Moreover, the narrow molecular weight distribution (M_w/M_n) was consistent in this copolymerization reaction.

The FTIR spectra of HPNFBC-*g*-P(SA-*alt*-BO) are presented in **Figure 1 (a)**. In the FTIR (ATR) spectra, HP-NFBC exhibited typical cellulose peaks at 3350 and 2890 cm^{-1} corresponding to the hydroxyl (O-H) and alkyl groups (C-H), respectively. After polymerization, HPNFBC-*g*-P(SA-*alt*-BO) exhibited a strong carbonyl (C=O) peak at 1723 cm^{-1}, which was attributed to the introduction of ester functional groups into HP-

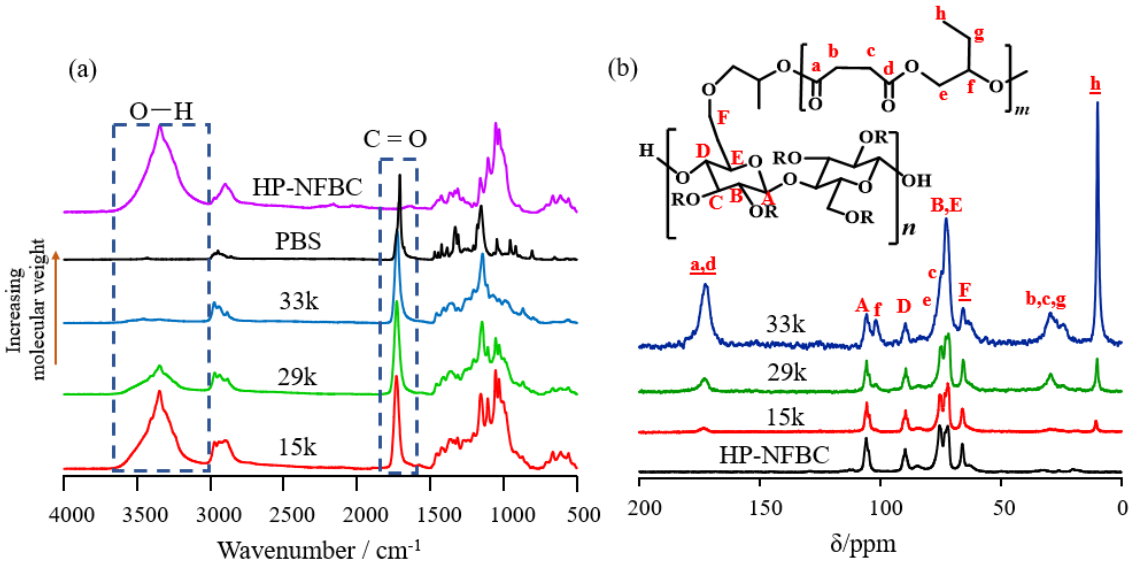

Figure 1 (a) FTIR (ATR) spectra of HP-NFBC, PBS, and HPNFBC-*g*-P(SA-*alt*-BO)s; respectively. **(b)** ^{13}C CP/MAS NMR spectra of HPNFBC-*g*-P(SA-*alt*-BO)s and HP-NFBC. ^{13}C CP/MAS NMR: ^{13}C cross-polarization magic- angle spinning nuclear magnetic resonance; ATR: attenuated total reflectance; FTIR: fourier-transform infrared; HP-NFBC: hydroxypropyl-nanofibrillated bacterial cellulose; PBS: polybutylene succinate

NFBC, indicating successful grafting of P(SA-*alt*-BO). The C=O peak was normalized to observe the difference in the absorbance of each hydroxyl group (O-H) peak. After normalization, the absorbance peak (y-axis) of O-H decreased as the molecular weight of the grafted copolymer increased. The FTIR results supported the increase in molecular weight of free copolymer in SEC analysis as more monomers were added. Notably, the amount of grafted copolymer was regulated by the amount of monomer feed. This has distinctly shown the efficiency of the grafting of P(SA-*alt*-BO) by "grafting-from" method.

Solid-state CP/MAS ^{13}C NMR measurements were performed on the HPNFBC-*g*-P(SA-*alt*-BO) samples to quantitatively determine the existence of cellulose backbone (HP-NFBC) and P(SA-*alt*-BO) ratio using the method proposed by Thongsomboon *et al* [45]. The coefficients corresponding to the non-overlapping peaks of anhydride [**Figure 1 (b); peak a, d**], epoxide [**Figure 1 (b); peak h**], and cellulose [**Figure 1(b); peak F**]

were calculated from the extrapolation of the semi-log linear approximation [**Figure S6 (b)**] derived from the Cross polarization (CP) time-relative magnetization graph [**Figure S6 (a)**]. The coefficients were obtained based on **eq. S5.** The molar ratio can be obtained by multiplying each coefficient by their corresponding ad, h, and F peaks, which represent SA, BO, and HP-NFBC, respectively. The quantitative composition of each compound is summarized in **Table S1**. The results showed that the cellulose content gradually decreased as the SA and BO contents increased, whereas HPNFBC-*g*-P(SA-*alt*-BO) (33k), which had the highest molecular weight, exhibited the lowest content of HP-NFBC. Moreover, the composition of SA and BO are similar to each other, indicating successful alternating copolymerization in this system, with no BO homopolymers grafted on the surface of HP-NFBC. In this study, the cellulose composition was adjusted based on this result for nanocomposite preparation.

AFM was conducted to compare the fiber morphologies of HPNFBC-*g*-P(SA-*alt*-BO) and non-grafted HP-NFBC. The HP-NFBC fiber was thin and clearly visible in both the height and phase images. The results were compared with those of HPNFBC-*g*-P(SA-*alt*-BO). The HPNFBC-*g*-P(SA-*alt*-BO) fibers appeared thicker, and shading and blurring were clearly observed along the fiber surface. In contrast, none of these were observed in HP-NFBC, indicating that the copolymer was successfully grafted onto the surface of HP-NFBC. The average fiber width was estimated by taking the average width from 50 spot measurements using ImageJ software; the average fiber widths of HP-NFBC and HPNFBC-*g*-P(SA-*alt*-BO) were 60 and 88 nm, respectively (**Figure S7**).

3.2. Characterization of nanocomposites prepared by solvent casted process

The mechanical properties of the PBS composites were examined by tensile testing. To demonstrate the advantage of the P(SA-*alt*-BO) grafting, we also prepared PBS nanocomposites with free copolymer P(SA-*alt*-BO) (M_n, 14,700; $Đ$, 1.37) as well as non-grafted HP-NFBC. The free copolymer P(SA-*alt*-BO) composite without cellulose exhibited the poorest mechanical properties, followed by non-grafted HP-NFBC [**Figure 2 (a)**]. In correlation with their morphological properties, defects in complete crystallization caused brittleness in non-grafted HP-NFBC because of poor dispersibility in the PBS matrix. However, when the copolymer was grafted onto HP-NFBC, the toughness and tensile strength increased remarkably **[Figure 2 (a), (c)]** because of the interaction of grafted copolymer with PBS matrix, in which the P(SA-*alt*-BO) chains act as an appropriate interface between the HP-NFBC and PBS. Moreover, the disordered structure of the amorphous grafted copolymer allowed for a greater elongation at break. While the lack of a crystal structure in amorphous polymers often leads to more ductile behavior, the addition of P(SA-*alt*-BO) to our nanocomposites led to an increase in the ultimate tensile strength because of its good interfacial compatibility with cellulose. When force was applied during the stretching, P(SA-*alt*-BO) acts as a plasticizer that facilitates the movement of PBS; at the same time, stress was transferred between cellulose resulting in the increase in tensile stress for the composite including 0.25 wt% HPNFBC-*g*-P(SA-*alt*-BO) (15k). A plasticizing effect was not observed in free copolymer addition because the chain head was not restricted to cellulose, causing slippage between chains without a strong grip at the end. In addition, non-grafted HP-NFBC has low impact resistance because of poor interfacial bonding with the PBS matrix.

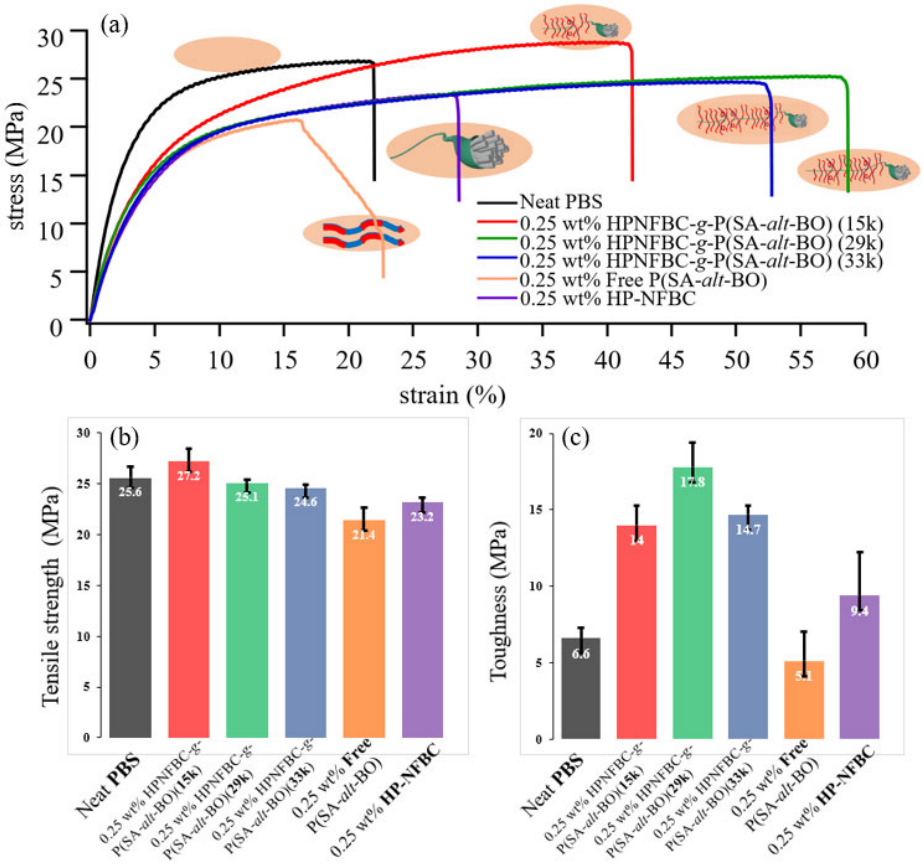

Figure 2 (a) Stress-strain curves of PBS (M_n, 44700; Đ, 2.2) and PBS nanocomposites **(b)** Tensile strength and toughness of PBS and PBS nanocomposite films at 0.25 wt% filler compositions. BO: 1,2-butylene oxide; SA: succinic anhydride; HP-NFBC: hydroxypropyl-nanofibrillated bacterial cellulose; PBS: polybutylene succinate

Furthermore, various types of nanocomposites were investigated to determine the effect of grafted copolymer on the mechanical properties of neat PBS [**Figure S8 (a)**]. First, composite materials containing various amounts of HPNFBC-g-P(SA-*alt*-BO) (15k) grafted with low-molecular-weight P(SA-*alt*-BO) were studied. Increasing the amount led to a declining trend in both the stress and strength. However, at the lowest incorporation at 0.25 wt%, the ultimate tensile strength and elongation at break exceeded the neat PBS by 106% (27.2 ± 1.3 MPa) and 202% (45.6 ± 6.2 MPa), respectively . The improvement in stress and strength with decreasing amounts of HPNFBC-*g*-P(SA-*alt*-BO) (15k) was due to the decreasing amorphous content; excess amorphous layer weakened the interaction between the cellulose and PBS matrix. Despite having

amorphous properties that can act as plasticizers to promote an increase in elongation at break, a smaller amount of P(SA-alt-BO) is preferable for stronger load transfer and higher toughness.

In addition, grafted NFBCs consisting of P(SA-*alt*-BO) with three different molecular weights were compared, and their effects on the mechanical properties were studied. The amount of HPNFBC-*g*-P(SA-*alt*-BO) was set to 0.25 wt%. As shown in **Figure S8 (b)**, higher molecular weight promoted an increase in the elongation at break. This further supported the use of the copolymer as a plasticizer. HPNFBC-*g*-P(SA-*alt*-BO) (33k) did not exhibit a higher elongation at break than 29k, potentially because 33k had a lower cellulose content to grip the head of the copolymer, which explains the slightly lower elongation during stretching. The tensile stress and Young's modulus decreased for longer chains because the HP-NFBC was largely covered by the long chains of P(SA-*alt*-BO), causing fracture to occur before the stress could be transferred within the cellulose **[Figure 2(b), (c)]**. A higher molecular weight results in increased elongation at break because of longer entanglement between chains, resulting in better load transfer between the copolymers; however, the decrease in cellulose content prevents them from having a higher ultimate tensile strength compared to the lesser molecular weight of the grafted copolymer. Overall, the addition of the graft copolymers increases the toughness of neat PBS, suggesting that the strength and toughness can be easily tuned by controlling the chain length and cellulose content.

Additionally, thermomechanical analysis of the nanocomposites was performed to measure the dimensional changes in the nanocomposites as a function of temperature to obtain their coefficient of thermal expansion (CTE). **Figures S9 (a) and (b)** represent the thermal expansion behavior of neat PBS and nanocomposites that contain 0.25 wt%

of HPNFBC-*g*-P(SA-*alt*-BO) with short (15k) and long (33k) copolymer chain length and comparison with neat PBS within the temperature range of 60–100℃. The addition of HPNFBC-*g*-P(SA-*alt*-BO) (15k) enhanced the thermal stability as evidenced by a 15.2% decrease in its CTE to 2.69 ppm/K compared to neat PBS (3.10 ppm/K). Conversely, higher CTE exhibited by HPNFBC-*g*-P(SA-*alt*-BO) (33k) (3.75 ppm/K) could be correlated with the smaller amount of HP-NFBC content and entanglement that makes it harder for the chain to expand freely as temperature rises, thus offering greater resistance to thermal expansion.

The original thermal behavior observed in the DSC 1st heating thermograms of the nanocomposites prepared by the solvent casting method was compared to that of neat PBS and is summarized in **Figure S10 (a)** and **Table S2**. First, the incorporation of the shortest HP-NFBC-grafted copolymer [HPNFBC-*g*-P(SA-*alt*-BO) (15k)] lowered the melting point, T_m of PBS. At this stage, the grafted copolymer with amorphous properties acts as a plasticizer, in which the intermolecular forces are reduced and the copolymer chain mobility increases. The decrease in T_m was due to an increase in chain mobility. Amorphous polymers are more prone to plasticization than crystalline polymers because of their random molecular arrangements and weaker intermolecular forces. This was also observed at a low crystallization temperature, T_c as indicated by the highest molecular weight HPNFBC-*g*-P(SA-*alt*-BO) (33k)/PBS. The uniformity of the PBS crystal did not change, as the sharpness of each crystallizing peak was similar, which was due to the small amount of grafted HP-NFBC present in each nanocomposite. Although HPNFBC-*g*-P(SA-*alt*-BO) (33k)/PBS had a lower crystallization temperature, it exhibited slightly higher crystallinity compared to the other grafted HP-NFBC and PBS implying higher nucleation rate which was further supported by polarized optical microscopy (POM)

results. As shown in **Figure S10 (d)**, the PBS chains slowly regained their mobility when lower compositions of HPNFBC-*g*-P(SA-*alt*-BO) (15k)/PBS were incorporated. As P(SA-*alt*-BO) is amorphous, the disordered molecular structure creates spaces between the PBS chains, which reduces intermolecular reactions, resulting in higher mobility because of less resistance to their movement.

The thermal stability of the nanocomposites was further investigated by thermogravimetry/differential thermal gravity (TG-DTG) analysis. TGA curves of neat PBS and all nanocomposites in **Figure S11 (a)** display a single weight loss step degradation at the range temperature of 260–430 °C that confirms no crosslinking in the nanocomposites. The onset of the decomposition temperature was determined by the temperature at 5% weight loss ($T_{5\%}$) and the highest derived weight loss curve (T_{max}) **[Figure S11 (b)]**. The addition of nanofiller did not result in any significant changes in the $T_{5\%}$ and T_{max} but maintained the thermal stability (**Table S3**).

POM analysis was conducted to analyze the dispersibility of the nanofillers in PBS. Neat PBS and three nanocomposites containing HPNFBC-*g*-P(SA-*alt*-BO), unmodified HP-NFBC, or free P(SA-*alt*-BO) copolymer, each at 0.25 wt% composition was used for the dispersibility analysis. The samples were heated above their melting temperature at 150 ℃ and kept constant for 5 min to observe the fibers. **Figure S12** shows POM images of neat PBS and its nanocomposites heated above the melting temperature. At 150 ℃, neat PBS and free copolymer P(SA-*alt*-BO) were fully melted and became transparent. In contrast, the fibers present in HPNFBC-P(SA-*alt*-BO)/PBS and HPNFBC/PBS became apparent as the PBS matrix melted. Non-surface-modified HP-NFBC showed a white cluster of fibers from the agglomeration in the PBS matrix due to the strong intermolecular and intramolecular hydrogen bonds and the incompatibility of

the hydrophilicity and hydrophobicity of the PBS matrix. However, after surface modification by grafting the P(SA-*alt*-BO) copolymer onto the surface of HP-NFBC, HP-NFBC showed uniform dispersibility in the PBS matrix. Grafting of the copolymer lowered the hydrophilicity of HP-NFBC, thus promoting compatibility with the PBS resin. The graft copolymers with higher molecular weights (29k and 33k) showed a smaller fiber size and higher dispersion compared to 15k.

The growth of the PBS crystals under isothermal conditions was observed using POM. P(SA-*alt*-BO) acts as a nucleation site because the nucleation rate and density appear to increase as the grafted copolymer length increases. HPNFBC-*g*-P(SA-*alt*-BO) (33k) had a higher nucleation rate and higher density of nucleation in some areas than that of neat PBS. This is consistent with the low crystallization temperature but higher crystallinity in DSC resulting from agglomeration. HPNFBC-*g*-P(SA-*alt*-BO) (15k) had a lower nucleation density and rate than that of neat PBS, resulting in broad empty spaces between the highly dense spherulites that later produced secondary crystallization. This secondary crystallization hindered the role of the amorphous copolymer as a plasticizer, leading to a decrease in the elongation at break. In contrast, a certain degree of crystallization enhancement is observed with the addition of non-grafted HP-NFBC, indicating that HP-NFBC itself has a function to promote crystallization. However, HP-NFBC was less dispersible in the PBS matrix and the nucleation density around the aggregated cellulose was lower. Moreover, crystallization was observed in unmodified HP-NFBC grown from the cellulose itself.

3.3. Characterization of nanocomposites prepared by melt-kneading process

Nanocomposites were also prepared by melt-kneading for a more practical evaluation of their physical properties. Only HPNFBC-*g*-P(SA-*alt*-BO) (15k) was selected because it exhibited the best mechanical properties when prepared by solvent-casting. Therefore, 0.25, 0.5, 2, and 5 wt% of HPNFBC-*g*-P(SA-*alt*-BO) (15k) were mixed with PBS and compared with neat PBS and non-grafted HP-NFBC mixed with PBS at 1, 3 and 5 wt% composition. The HP-NFBC content in HPNFBC-g-P(SA-alt-BO) (15k) at 0.25, 0.5, 2, and 5 wt% were 0.1, 0.25, 1.0 and 1.9 wt% respectively. The nanocomposites prepared via melt-kneading were subjected to three-point bending test. In this test, modulus of elasticity in bending E_f, flexural stress σ_f, flexural strain ε_f as well as the Young's modulus can be obtained. This test is especially important for determining the modulus of elasticity or flexural modulus that characterizes a nanocomposite's stiffness or resistance to bending that is closer to real-life applications. The results of the flexural tests of the nanocomposites prepared by melt kneading are presented in **Figure S13**. The flexural test results showed that the addition of HPNFBC-*g*-P(SA-*alt*-BO) and HP-NFBC increased both the ultimate flexural strength and Young's modulus. Interestingly, at only 0.25 wt% of HPNFBC-*g*-P(SA-*alt*-BO), the elastic modulus (stiffness) has increased to 7.5% and continued to increase to 12.9% at 2 wt% incorporation of HPNFBC-*g*-P(SA-*alt*-BO). This indicates that the melt-kneading method provided better dispersion of the HPNFBC-*g*-P(SA-*alt*-BO) nanoparticles within the PBS matrix, resulting in improved alignment and distribution, which contributed to the increase in its Young's modulus. In addition to the good dispersion provided by the melt-kneading process, modification of the hydrophobic copolymer P(SA-*alt*-BO) on the surface of HP-NFBC increased its compatibility and further improved its dispersion within the PBS matrix. To compare the amount of cellulose (HP-NFBC) in each sample,

374 at 0.75 wt% of cellulose content in HPNFBC-*g*-P(SA-*alt*-BO), the ultimate flexural
375 strength was higher by 2.6% than that of HP-NFBC at 1 wt%. Initially, HPNFBC-*g*-P(SA-
376 *alt*-BO) exhibited enhanced mechanical properties compared to HP-NFBC, but with 5
377 wt% addition of HPNFBC-*g*-P(SA-*alt*-BO) containing 1.8 wt% cellulose content, while
378 the elastic modulus continued to increase, the flexural strength suddenly decreased at high
379 HPNFBC-*g*-P(SA-*alt*-BO) content. This decrease in tensile strength may be attributed to
380 agglomeration, a phenomenon previously observed in solvent-cast nanocomposite films.

381 **3.4. The effect of thermal annealing**

382 Thermal annealing is an effective post-treatment method for adjusting the crystallinity of
383 semi-crystalline polymers. Therefore, the mechanical properties and crystallization
384 behavior of the melt-kneaded nanocomposites were investigated to promote their
385 industrial application. All the respective nanocomposites were annealed at 80 ℃, under
386 vacuum for 16h. The tensile test results for the melt-kneaded films after annealing are
387 shown in **Figure 3 (a)**. In contrast, **Figure 3 (b)** shows the comparison between grafted
388 and non-grafted HP-NFBC at the same 1 wt% cellulose content. Moreover, 2 wt% loading
389 of HPNFBC-*g*-P(SA-*alt*-BO) (15k) that contains 1 wt% of HP-NFBC has high strength
390 and toughness than that of neat PBS. In contrast, the 1 wt% of non-grafted HP-NFBC
391 exhibited similar ultimate tensile strength but lower toughness owing to the absence of
392 plasticizing properties. The grafting of P(SA-*alt*-BO) increases the elongation at break
393 while maintaining the tensile strength provided by HP-NFBC. After annealing, the
394 Young's modulus of neat PBS was increased by 39% from 291 MPa to 405 MPa.
395 Furthermore, the increase in Young's modulus after 2 wt% of HPNFBC-*g*-P(SA-*alt*-BO)
396 addition was 30.5% **(Figure S14).** The increase in Young's modulus after thermal

annealing indicates a more ordered and stable polymer chain structure that aligns more uniformly, which contributes to the stiffness of the films. The elongation at break of the nanocomposites, especially at 1 and 0.1 wt%, exceeded the elongation at break of neat PBS, unlike the non-annealed nanocomposites, which exhibited lower elongation at break compared to neat PBS. The reorganization of polymer chains during heating and cooling due to thermal annealing led to an improvement in the rearrangement of P(SA-*alt*-BO) in the PBS matrix, which further enhanced the plasticizing effect of the amorphous polymer.

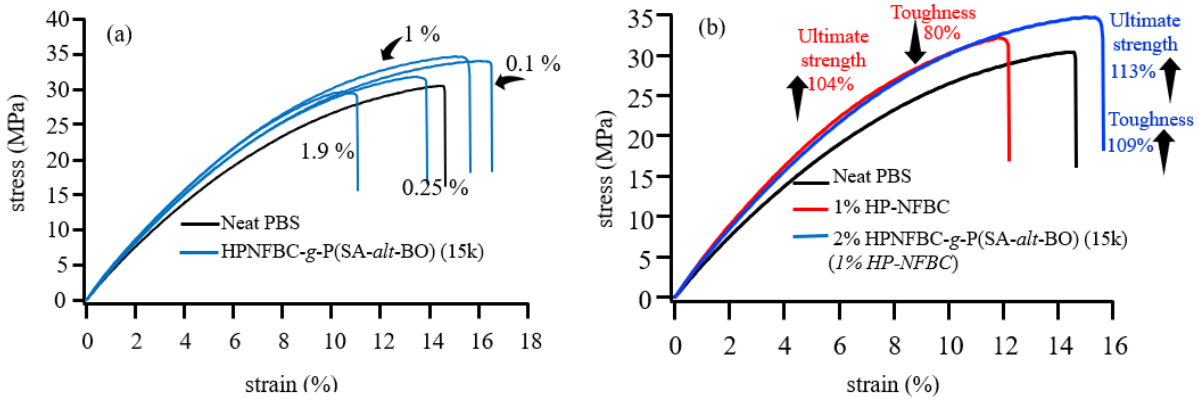

Figure 3 (a) Stress-strain curves of neat PBS and HPNFBC-*g*-P(SA-*alt*-BO)/PBS at various compositions after annealing treatments. **(b)** Comparison between mechanical properties of grafted and non-grafted HP-NFBC at the same 1 wt% cellulose content after annealing treatments. BO: 1,2-butylene oxide; SA: succinic anhydride; HP-NFBC: hydroxypropyl-nanofibrillated bacterial cellulose; PBS: polybutylene succinate

The thermal properties of the melt-kneaded and annealed nanocomposites were investigated using DSC [**Figures 4 (a) and (b)**]. During the 1st heating and 1st cooling, there was only a minor change in the melting temperature when HPNFBC-*g*-P(SA-*alt*-BO) was added, probably owing to its small composition. Unlike the solvent-cast nanocomposites, slight increases in T_m were observed at 0.1, 0.25, and 1 wt% incorporation of filler. The homogenous dispersion of HPNFBC-*g*-P(SA-*alt*-BO) was attributed to the melt-kneading process and improved chain alignment during recrystallization via thermal annealing. A significant change can be observed in the

integrated area representing the energy of fusion, where the nanocomposites exhibit a higher surface area, indicating a higher degree of crystallinity.

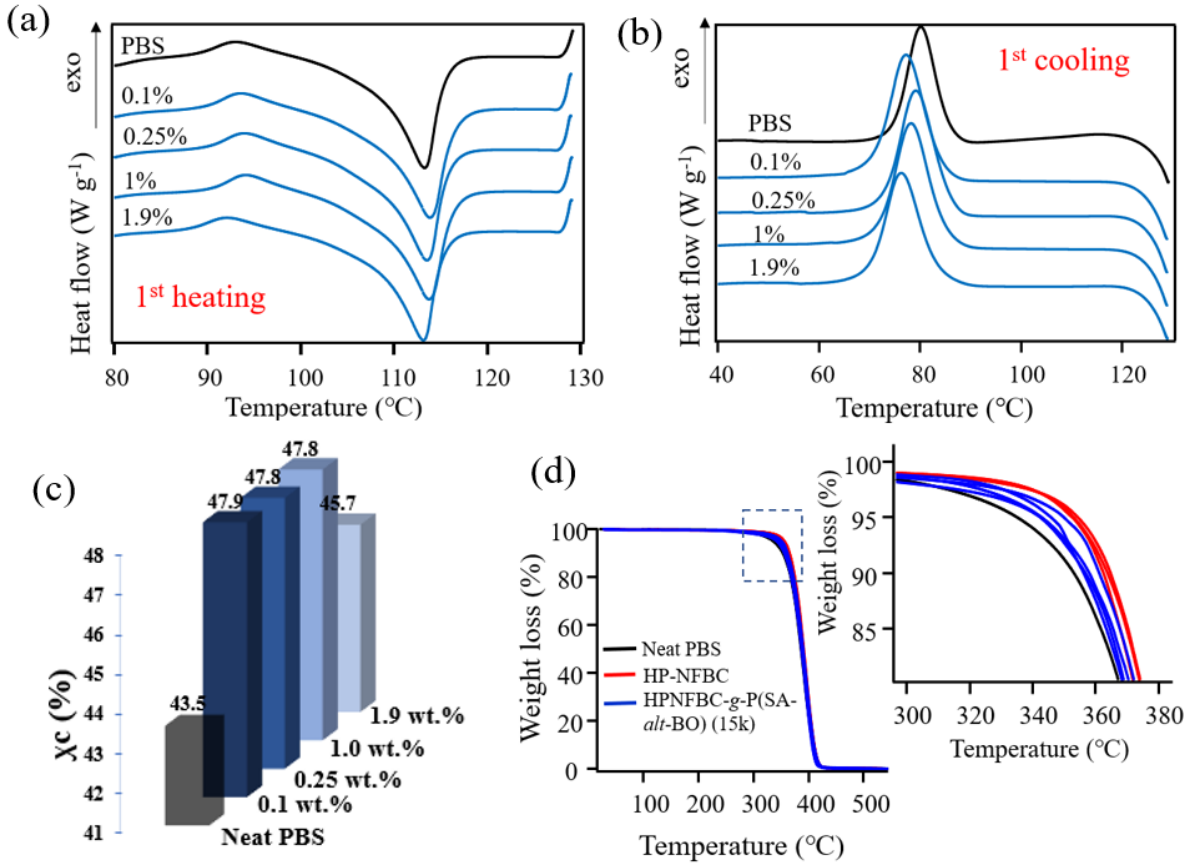

Figure 4 (a) 1st heating **(b)** 1st cooling thermograms of nanocomposites with different compositions of annealed HPNFBC-*g*-P(SA-*alt*-BO) (15k). Each thermogram was compared with annealed neat PBS (M*n* 44700; *Đ*, 2.2). **(c)** Crystallinity [χc (%)] of HPNFBC-*g*-P(SA-*alt*-BO)(15k)/PBSs and neat PBS after annealing treatments. **(d)** TGA curves for neat PBS, non-grafted HP-NFBC and HPNFBC-*g*-P(SA-*alt*-BO) (15 k), respectively after annealed.

Moreover, the 1st cooling thermograms support the increase in crystallization activity, as all crystals in the nanocomposites grew at lower temperatures than in neat PBS. The increase in crystallinity can be related to the amorphous properties of the copolymer, which are flexible and mobile; when blended with semi-crystalline PBS, they increase the PBS chain mobility. The crystallinity slowly showed a decreasing trend at higher grafted-copolymer contents because too much amorphous content could disrupt the crystalline order and reduce the crystallinity [**Figure 4 (c)**]. This further supports the

poor mechanical properties of the nanocomposites with higher loadings of the grafted copolymer.

Table 2 Degradation temperature at 5% ($T_{5\%}$) and 50% ($T_{50\%}$) weight loss for each sample after annealing treatments.

Sample	wt% of HP-NFBC	$T_{5\%}$ (°C)[a]	$T_{50\%}$ (°C)[b]
Neat PBS	-	335.4	386.6
HP-NFBC /PBS	1	354.6	391.0
	3	353.1	391.0
	5	352.6	390.0
HPNFBC-*g*-P(SA-*alt*-BO)(15k) /PBS	0.1	346.1	390.2
	0.25	343.1	388.5
	1	350.2	390.0
	1.9	342.6	387.2

[a]Temperature at 5% weight loss. [b]Temperature at 50% weight loss.

The thermal stability of the nanocomposite samples was analyzed using TGA [**Figure 4 (d)**]. Despite the lower loading of filler in both grafted and non-grafted HP-NFBC loaded nanocomposites, the $T_{5\%}$ and $T_{50\%}$ degradation temperature significantly increased from 7.2 to 19.2 ℃ and 0.6 to 4.4 ℃ , respectively (**Table 2**). Films with grafted HP-NFBC had a slightly lower degradation temperature than that of non-grafted HP-NFBC because the introduction of amorphous P(SA-*alt*-BO) disrupts the regular packing of the HP-NFBC chains, resulting in less energy to undergo thermal degradation. The amorphous regions, which refer to the grafted copolymer, generally have weaker intermolecular forces, resulting in a slight reduction in the thermal degradation temperature. However,

both the grafted and non-grafted HP-NFBC exhibited higher degradation temperatures than that of neat PBS.

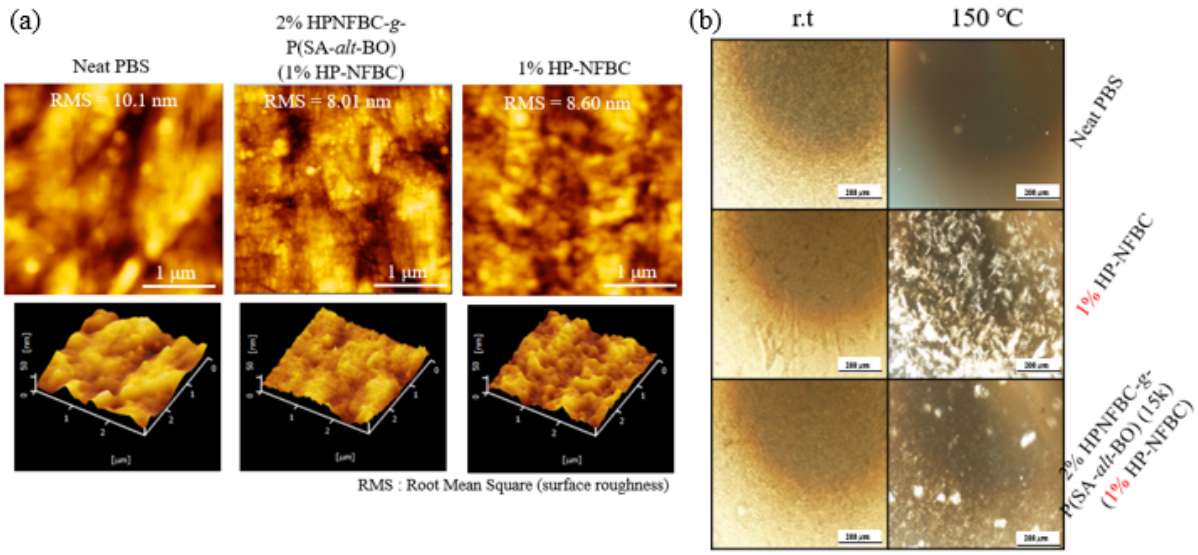

Figure 5 (a) Surface roughness of neat PBS compared to grafted and non-grafted HP-NFBC assessed using atomic force microscopy (AFM). **(b)** Dispersibility assessment using polarized optical microscopy (POM).

AFM was used to evaluate the morphological properties of the annealed neat PBS and grafted and non-grafted HP-NFBC. The surface roughness due to the addition of HPNFBC-*g*-P(SA-*alt*-BO) nanofillers [**Figure 5 (a)**] was lower than that of neat PBS, indicating that it had fewer irregularities and smoother features. This is because of the more homogenous distribution of HPNFBC-*g*-P(SA-*alt*-BO), which fills the gaps or irregularities within the PBS matrix. Moreover, these results are correlated with the improvement in PBS alignment, which aided in increased crystallinity. Furthermore, non-grafted HP-NFBC showed lower surface roughness; however, a smoother surface was observed after grafting with P(SA-*alt*-BO) copolymer showing that better interactions can be achieved by grafting hydrophobic moieties. The dispersibility of the nanofillers was investigated using POM to further evaluate the surface roughness. **Figure 5 (b)** shows the dispersibility of neat PBS and the nanocomposites with grafted and non-grafted HP-

NFBC at the same cellulose content (1 wt% of HP-NFBC). The films were observed at room temperature and 150 ℃. At 150 ℃, the PBS had completely melted and the fibers that did not melt remained visible and the dispersibility was observable. Based on these results, the fibers in the grafted and non-grafted HP-NFBC were evenly distributed throughout the entire matrix; however, the non-grafted HP-NFBC showed more clumps or aggregation than the P(SA-*alt*-BO)-grafted HP-NFBC. In contrast, HPNFBC-*g*- P(SA-*alt*-BO), which has a similar 1 wt% cellulose fiber content, exhibits much less aggregation, demonstrating the effectiveness of grafting hydrophobic moieties onto the surface of HP-NFBC.

3.5. Biodegradability test

A simple biodegradation test was performed by 90-days soil burial test to evaluate the biodegradation rates of the nanocomposite materials. Potting soil containing organic matter, microorganisms, and moisture was used as the medium for biodegradation. The burial samples were incubated at 25 ℃, which is the appropriate temperature for breakdown of the organic matter by microorganisms. The appearance of the samples on the first day and after 90 d are shown in **Figure 6 (a)**. The percentage weight loss was subtle in each sample and showed no noticeable difference between the grafted and non-grafted HP-NFBC and neat PBS as well **[Figure 6 (b)]**. This suggests that the modification of HP-NFBC and its addition had little effect on the biodegradation activity of PBS. In addition, the preservation of biodegradability is favorable for environmental sustainability. No apparent changes were observed before and after 90 d, but scanning electron microscopy (SEM) revealed the activity of microorganisms **[Figure 6 (c)]**. After 90 d, increase in porosity of HPNFBC-*g*-P(SA-*alt*-BO) (1 wt%) was observed due to

microbial degradation. A microporous structure was observed in all the samples after 90 d **[Figure 6 (d)]**.

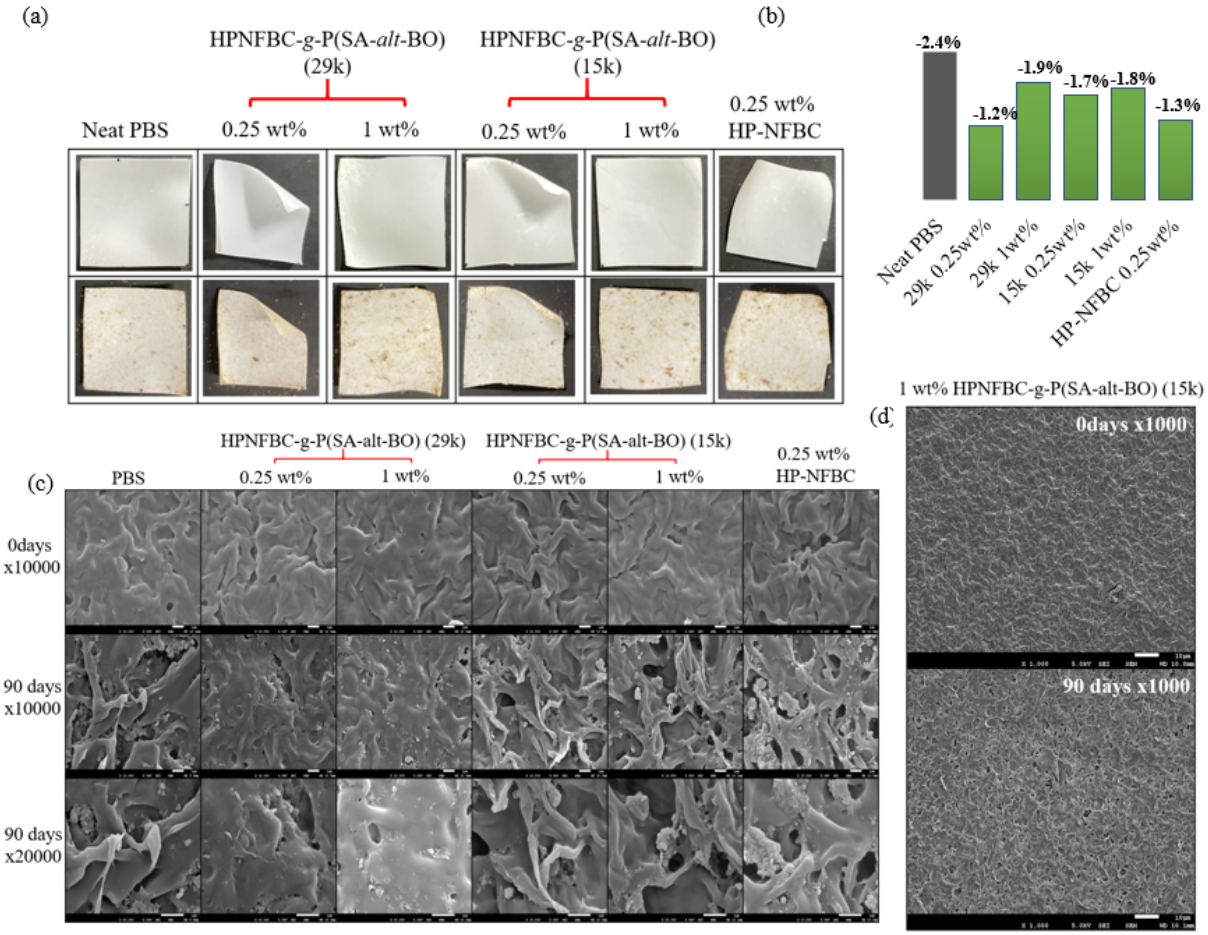

Figure 6 (a) Images of biodegradable test samples on days 0 (upper) and 90 (lower). **(b)** Change in sample weight after 90 d. **(c)** SEM images of films before and after biodegradation testing **(d)** Existence of holes after 90 d.

Conclusions

HP-NFBC, an environmentally friendly polymeric material prepared from low-molecular-weight biomass such as carbohydrates, was successfully modified by HPNFBC-*g*-P(SA-*alt*-BO) grafting through the SI-ROCOP of SA and BO, initiated from the abundant hydroxyl groups on the surface of HP-NFBC. This grafting method provided an efficient way to control the molecular weight of the copolymers by controlling the initial ratio of monomers and initiators. The grafting of P(SA-*alt*-BO) onto HP-NFBC

showed a marked advantage in terms of dispersion and mechanical properties in the PBS matrix compared with unmodified HP-NFBC films prepared using both solvent-casting and melt-kneading. Additionally, thermal annealing of the melt-kneaded nanocomposites contributed to an increase in both the stiffness and toughness compared with the non-thermally treated films. Nanocellulose exhibit rigid and strong properties; thus, adding nanocellulose into a polymer matrix often causes an increase in tensile strength and decrease in elongation at break, resulting in stiffer material. However, our nanocomposite exhibits high toughness because of the amorphous property of grafted P(SA-*alt*-BO) that that act as a plasticizer, contributing to the more ductile behavior, hence, the increase in elongation at break. Moreover, the existence of cellulose helps to maintain the tensile strength. The mechanical properties of composites containing grafted HP-NFBC can be easily tuned by controlling the molecular weight of the grafted polymer, cellulose content, and nanocomposite preparation methods, providing more options for their application. In addition, composites containing grafted HP-NFBC have the added value of being biodegradable, and further development of composites is expected in the future.

Supporting Information

^{1}H NMR spectra of all samples; SEC traces; AFM images; stress-strain curves from tensile tests of solvent-cast nanocomposites; TG-DTG curves; and stress-strain curves from flexural and tensile tests of melt-kneaded nanocomposites.

Funding

This work was financially supported by the JSPS Grant-in-Aid for Scientific Research (B) (No. 19H02549, K.T.).

Acknowledgement

We thank Dr. Yuki Kugo, Dr. Satoshi Nomura, Mr. Naoya Nakagawa, and Prof. Tomoki Erata of Hokkaido University for their support with NMR measurements. The authors further thank Mr. Kenji Ohkubo of Hokkaido University for his assistance with SEM observations. This work was supported by the Hokkaido University Research and Education Center for Robust Agriculture, Forestry, and Fisheries Industry, and the JST-Mirai Program (Grant Number JPMJMI21EE).

Author contributions

Hamidah binti Hashim: Methodology, Experiments, Analysis, Writing. Xiaochao Xia: Methodology. Hiroshi Kani: Methodology, Experiments. Shuichiro Seno: Methodology, Experiments. Li Feng: Methodology. Takuya Isono: Supervision. Takuya Yamamoto: Supervision. Hirofumi Tani: Supervision. Toshifumi Satoh: Supervision. Kenji Tajima: Conceptualization, Methodology, Supervision, Writing – Review and Editing, Funding acquisition, Project administration

Conflict of Interests

The authors declare that they have no financial or personal relationships that may be considered as potential competing interests.

Data availability

Data will be made available on request.

Abbreviations

NFBC, nanofibrillated bacterial cellulose; PBS, polybutylene succinate; HPC, hydroxypropyl cellulose; FT-IR, Fourier-transform infrared; NMR, nuclear magnetic resonance; SEC, size-exclusion chromatography; DSC, differential scanning calorimetry;

TG-DTG, thermogravimetry/differential thermal gravity analysis; AFM, atomic force microscopy; POM, polarized optical microscopy; TMA, thermomechanical analysis; CTE, coefficient of thermal expansion.

References

[1] El-Hadi A, Schnabel R, Straube E, Müller G, Henning S. Correlation between degree of crystallinity, morphology, glass temperature, mechanical properties and biodegradation of poly (3-hydroxyalkanoate) PHAs and their blends. Polymer Testing 2002;21:665–74. https://doi.org/10.1016/S0142-9418(01)00142-8.

[2] Pan Y, Farmahini-Farahani M, Hearn PO, Xiao H, Ocampo H. An overview of bio-based polymers for packaging materials. Journal of Bioresources and Bioproducts 1996;1:106–13. https://doi.org/10.21967/jbb.v1i3.49.

[3] Petersen K, Nielsen PV., Olsen MB. Physical and mechanical properties of biobased materials - Starch, polylactate and polyhydroxybutyrate. Starch/Stärke 2001;53:356–61. https://doi.org/10.1002/1521-379X(200108)53:8<356::AID-STAR356>3.0.CO;2-7.

[4] Storz H, Vorlop KD. Bio-based plastics: Status, challenges and trends. Landbauforschung Volkenrode 2013;63:321–32. https://doi.org/10.3220/LBF-2013-321-332.

[5] Yatigala NS, Bajwa DS, Bajwa SG. Compatibilization improves physico-mechanical properties of biodegradable biobased polymer composites. Composites Part A: Applied Science and Manufacturing 2018;107:315–25. https://doi.org/10.1016/j.compositesa.2018.01.011.

[6] Zengwen C, Pan H, chen Y, Bian J, Han L, Zhang H, et al. Transform poly (lactic acid) packaging film from brittleness to toughness using traditional industrial equipments. Polymer 2019;180:121728. https://doi.org/10.1016/j.polymer.2019.121728.

[7] Zhao G, Gomes FPC, Marway H, Thompson MR, Zhu Z. Physical aging as the driving force for brittle–ductile transition of polylactic acid. Macromolecular Chemistry and Physics 2020;221:1–9. https://doi.org/10.1002/macp.201900475.

[8] Hu M, Deng C, Gu X, Fu Q, Zhang J. Manipulating the strength-toughness balance of poly(l-lactide) (PLLA) via introducing ductile poly(ϵ-caprolactone) (PCL) and strong shear flow. Industrial and Engineering Chemistry Research 2020;59:1000–9. https://doi.org/10.1021/acs.iecr.9b05380.

[9] Katsumata K, Saito T, Yu F, Nakamura N, Inoue Y. The toughening effect of a small amount of poly(ε-caprolactone) on the mechanical properties of the poly(3-hydroxybutyrate-co-3-hydroxyhexanoate)/PCL blend. Polymer Journal 2011;43:484–92. https://doi.org/10.1038/pj.2011.12.

[10] Chan CM, Pratt S, Halley P, Richardson D, Werker A, Laycock B, et al. Mechanical and physical stability of polyhydroxyalkanoate (PHA)-based wood plastic composites (WPCs) under natural weathering. Polymer Testing 2019;73:214–21. https://doi.org/10.1016/j.polymertesting.2018.11.028.

582 [11] Chen GQ, Chen XY, Wu FQ, Chen JC. Polyhydroxyalkanoates (PHA) toward cost
583 competitiveness and functionality. Advanced Industrial and Engineering Polymer
584 Research 2020;3:1–7. https://doi.org/10.1016/j.aiepr.2019.11.001.

585 [12] Rafiqah SA, Khalina A, Harmaen AS, Tawakkal IA, Zaman K, Asim M, et al. A review
586 on properties and application of bio-based poly (butylene succinate). Polymers 2021;13:1–
587 28. https://doi.org/10.3390/polym13091436.

588 [13] Tserki V, Matzinos P, Pavlidou E, Vachliotis D, Panayiotou C. Biodegradable aliphatic
589 polyesters. Part I. Properties and biodegradation of poly (butylene succinate-co-butylene
590 adipate). Polymer Degradation and Stability 2006;91:367 –76.
591 https://doi.org/10.1016/j.polymdegradstab.2005.04.035.

592 [14] Xu J, Guo BH. Poly (butylene succinate) and its copolymers : Research , development and
593 industrialization. Biotechnology Journal 2010;5:1149–63.
594 https://doi.org/10.1002/biot.201000136.

595 [15] Fujimaki T. Processability and properties of aliphatic polyesters, 'BIONOLLE',
596 synthesized by polycondensation reaction. Polymer Degradation and Stability
597 1998;59:209–14. https://doi.org/10.1016/s0141-3910(97)00220-6.

598 [16] Vytejčková S, Vápenka L, Hradecký J, Dobiáš J, Hajšlová J, Loriot C, et al. Testing of
599 polybutylene succinate based films for poultry meat packaging. Polymer Testing
600 2017;60:357–64. https://doi.org/10.1016/j.polymertesting.2017.04.018.

601 [17] Siracusa V, Lotti N, Munari A, Dalla Rosa M. Poly(butylene succinate) and poly(butylene
602 succinate-co-adipate) for food packaging applications: Gas barrier properties after stressed
603 treatments. Polymer Degradation and Stability 2015;119:35–45.
604 https://doi.org/10.1016/j.polymdegradstab.2015.04.026.

605 [18] Petchwattana N, Covavisaruch S, Wibooranawong S, Naknaen P. Antimicrobial food
606 packaging prepared from poly(butylene succinate) and zinc oxide. Measurement: Journal
607 of the International Measurement Confederation 2016;93:442–8.
608 https://doi.org/10.1016/j.measurement.2016.07.048.

609 [19] Ayu RS, Khalina A, Harmaen AS, Zaman K, Mohd Nurrazi N, Isma T, et al. Effect of
610 empty fruit brunch reinforcement in polybutylene-succinate/modified tapioca starch blend
611 for agricultural mulch films. Scientific Reports 2020;10:1–7.
612 https://doi.org/10.1038/s41598-020-58278-y.

613 [20] Bo L, Guan T, Wu G, Ye F, Weng Y. Biodegradation behavior of degradable mulch with
614 poly (butylene adipate-co-terephthalate) (PBAT) and poly (butylene succinate) (PBS) in
615 simulation marine environment. Polymers 2022;14:1515.
616 https://doi.org/10.3390/polym14081515.

617 [21] Fortunati E, Puglia D, Iannoni A, Terenzi A, Kenny JM, Torre L. Processing conditions,
618 thermal and mechanical responses of stretchable poly (lactic acid)/poly (butylene
619 succinate) films. Materials 2017;10:809. https://doi.org/10.3390/ma10070809.

620 [22] Bhatia A, Gupta RK, Bhattacharya SN, Choi HJ. Compatibility of biodegradable poly
621 (lactic acid) (PLA) and poly (butylene succinate) (PBS) blends for packaging application.
622 Korea-Australia Rheology Journal 2007;19:125–31.

[23] Deng Y, Thomas NL. Blending poly(butylene succinate) with poly(lactic acid): Ductility and phase inversion effects. European Polymer Journal 2015;71:534–46. https://doi.org/10.1016/j.eurpolymj.2015.08.029.

[24] Adrar S, Ajji A. Effect of blending sequence and epoxy functionalized compatibilizer on barrier and mechanical properties of PBS and PBS/PLA nanocomposite blown films. Journal of Vinyl and Additive Technology 2024. https://doi.org/10.1002/vnl.22092.

[25] Li J, Wang X, Li Y, Hu H, Liang X. Rheological, thermal, and mechanical properties of poly(butylene succinate) (PBS)/poly(L-lactide) (PLA) fiber biodegradable green composites. Colloid and Polymer Science 2024:1–14. https://doi.org/10.1007/s00396-024-05243-0.

[26] Kiziltas A, Nazari B, Kiziltas EE, Gardner DJS, Han Y, Rushing TS. Cellulose NANOFIBER-polyethylene nanocomposites modified by polyvinyl alcohol. Journal of Applied Polymer Science 2016;133:1–8. https://doi.org/10.1002/app.42933.

[27] Li K, Mcgrady D, Zhao X, Ker D, Tekinalp H, He X, et al. Surface-modified and oven-dried microfibrillated cellulose reinforced biocomposites: Cellulose network enabled high performance. Carbohydrate Polymers 2021;256:117525. https://doi.org/10.1016/j.carbpol.2020.117525.

[28] Li Y, Chen C, Xu J, Zhang Z, Yuan B, Huang X. Improved mechanical properties of carbon nanotubes-coated flax fiber reinforced composites. Journal of Materials Science 2015;50:1117–28. https://doi.org/10.1007/s10853-014-8668-3.

[29] Platnieks O, Sereda A, Gaidukovs S, Thakur VK, Barkane A, Gaidukova G, et al. Adding value to poly (butylene succinate) and nanofibrillated cellulose-based sustainable nanocomposites by applying masterbatch process. Industrial Crops Prod 2021;169:113669. https://doi.org/10.1016/j.indcrop.2021.113669.

[30] Kose R, Sunagawa N, Yoshida M, Tajima K. One-step production of nanofibrillated bacterial cellulose (NFBC) from waste glycerol using Gluconacetobacter intermedius NEDO-01. Cellulose 2013;20:2971–9. https://doi.org/10.1007/s10570-013-0050-0.

[31] Kono H, Uno T, Tsujisaki H, Anai H, Kishimoto R, Matsushima T, et al. Nanofibrillated bacterial cellulose surface modified with methyltrimethoxysilane for fiber-reinforced composites. ACS Applied Nano Materials 2020;3:8232–41. https://doi.org/10.1021/acsanm.0c01670..

[32] Kono H, Uno T, Tsujisaki H, Matsushima T, Tajima K. Nanofibrillated bacterial cellulose modified with (3-aminopropyl)trimethoxysilane under aqueous conditions: Applications to poly(methyl methacrylate) fiber-reinforced nanocomposites. ACS Omega 2020;5:29561–9. https://doi.org/10.1021/acsomega.0c04533.

[33] Tajima K, Kusumoto R, Kose R, Kono H, Matsushima T, Isono T, et al. One-step production of amphiphilic nanofibrillated cellulose using a cellulose-producing bacterium. Biomacromolecules 2017;18:3432–8. https://doi.org/10.1021/acs.biomac.7b01100.

[34] Hashim HB, Emran NAAB, Isono T, Katsuhara S, Ninoyu H, Matsushima T, et al. Improving the mechanical properties of polycaprolactone using functionalized nanofibrillated bacterial cellulose with high dispersibility and long fiber length as a

reinforcement material. Composites Part A: Applied Science and Manufacturing 2022;158:106978. https://doi.org/10.1016/j.compositesa.2022.106978.

[35] Xia W, Qin X, Zhang Y, Sinko R, Keten S. Achieving enhanced interfacial adhesion and dispersion in cellulose nanocomposites via amorphous interfaces. Macromolecules 2018;51:10304–11. https://doi.org/10.1021/acs.macromol.8b02243.

[36] Soeta H, Lo Re G, Masuda A, Fujisawa S, Saito T, Berglund LA, et al. Tailoring nanocellulose-cellulose triacetate interfaces by varying the surface grafting density of poly(ethylene glycol). ACS Omega 2018;3:11883–9. https://doi.org/10.1021/acsomega.8b01616.

[37] Vega-hernández MÁ, Cano-díaz GS, Vivaldo-lima E, Rosas-aburto A, Hernández-luna MG, Martinez A, et al. A review on the synthesis, characterization and modeling of polymer grafting. Processes 2021;9:1–85. https://doi.org/10.3390/pr9020375.

[38] Xia X, Suzuki R, Takojima K, Jiang DH, Isono T, Satoh T. Smart access to sequentially and architecturally controlled block polymers via a aimple catalytic polymerization system. ACS Catalysis 2021;11:5999–6009. https://doi.org/10.1021/acscatal.1c00382.

[39] Wang H, Roeder RD, Whitney RA, Champagne P, Cunningham MF. Graft modification of crystalline nanocellulose by Cu (0)-mediated SET living radical polymerization. Journal of Polymer Science Part A: Polymer Chemistry 2015;53:2800–8. https://doi.org/10.1002/pola.27754.

[40] Rosilo H, McKee JR, Kontturi E, Koho T, Hytönen VP, Ikkala O, et al. Cationic polymer brush-modified cellulose nanocrystals for high-affinity virus binding. Nanoscale 2014;6:11871–81. https://doi.org/10.1039/c4nr03584d.

[41] Wohlhauser S, Rader C, Weder C. Facile method to determine the molecular weight of polymer grafts grown from cellulose nanocrystals. Biomacromolecules 2022;23:699–707. https://doi.org/10.1021/acs.biomac.1c01050.

[42] Roy BLF, Heinrich LA, Tayo LL, Malmström E, Engström J. Grafting of poly(ε-caprolactone) from Abaca cellulose fibers via ring-opening polymerization resulting in facile one-pot biocomposites. SPE Polymers 2021;2:297–310. https://doi.org/10.1002/pls2.10058.

[43] Olsén P, Herrera N, Berglund LA. Polymer grafting inside wood cellulose fibers by improved hydroxyl accessibility from fiber swelling. Biomacromolecules 2020;21:597–603. https://doi.org/10.1021/acs.biomac.9b01333.

[44] Lönnberg H, Fogelström L, Berglund L, Malmström E, Hult A. Surface grafting of microfibrillated cellulose with poly(ε-caprolactone)–Synthesis and characterization. European Polymer Journal 2008;44:2991–7. https://doi.org/10.1016/j.eurpolymj.2008.06.023.

[45] Thongsomboon W, Serra DO, Possling A, Hadjineophytou C, Hengge R, Cegelski L. Phosphoethanolamine cellulose: A naturally produced chemically modified cellulose. Science 2018;359:334–8